Modeling Agglomeration of Nano-Particles in Molecular Dynamics (MD) Software

Gizem Inci

Institute for Combustion Technology, University of Stuttgart, Herdweg 51, 70174 Stuttgart, Germany

November 21, 2012

Project Coordinator: Prof. Dr. Andreas Kronenburg
Project Co-Advisor: JP Dr. Axel Arnold
Project Title: Agglomeration of Nanosized Particles in Turbulent Flows
Project Start: 01.01.2011

1 INTRODUCTION

Particle agglomeration is an abundant process in nature and in many industrial processes such as spray drying and particle flame synthesis but also in water purification, mineral benification and biological separation processes [1, 2]. Agglomeration is a mass conserving growth mechanism that starts after the primary particles (sized between 1 nm and 100 nm) are formed by nucleation and surface growth. Usually the particles are dispersed in a fluid (liquid or gas) and the agglomeration phenomenon can be driven both by the flow process and/or by Brownian motion that induce relative motion of the particles [3–5]. Due to their relative motion, the particles collide and adhere when the net interparticle attractive force overcomes the thermal agitation and the hydrodynamic drag [6, 7]. The composition of irregular clusters of the collided particles with different sizes and shapes depends on the specific formation and growth mechanisms and we need either experimental methods or computer simulations to obtain quantitative information on the respective mechanisms that govern the agglomeration process.

In our study, we seek an MD simulation algorithm to model the particle agglomeration in which the collided particles remain fixed at the initial point of contact. Different algorithms are developed (Table 2) that are based on either the van der Waals interparticle forces or bonding forces or on additional external point particles to inhibit the particle sliding away from the first contact point during the MD simulations. The Brownian motion of the interacting particles are modeled by solving the Langevin equation of motion and the particle interactions are taken to be a Lennard-Jones intermolecular potential assuming all primary particles are spherical and have the same (known) diameter.

The paper begins with a description of the numerical solver including a theoretical account of the intermolecular potential and the Langevin equation for Brownian particles. The paper continues in Section 3 with an investigation and comparison of the fractal and morphological properties of the nanoparticle agglomerates for each model. The accomplished model is selected by evaluating the results of these different algorithms.

2 NUMERICAL METHODS

2.1 Interactions

The flexible Molecular Dynamics (MD) software package ESPResSo [8] is used to perform the numerical simulations. The traditional (12-6) Lennard-Jones potential between particles is used to model interactions between non-polar molecules. It combines a long-range attractive force (the $1/r^6$ term) with a short-range repulsive force (the $1/r^{12}$ term) between the particles,

$$V_{LJ}(r) = \begin{cases} 4\epsilon \left(\left(\frac{\sigma}{r}\right)^{12} - \left(\frac{\sigma}{r}\right)^{6} + c_{shift} \right) & \text{, if } r_{min} < r < r_{cut} \\ 0 & \text{, otherwise} \end{cases} \tag{1}$$

where σ is the radius of the primary particle, ϵ is the depth of the attractive potential, defining the maximum attractive energy between two particles. The attraction between the particles starts beyond the value of $r = 2^{1/6}\sigma$. The

potential becomes continuous at the cut-off radius r_{cut} if $c_{shift} = \left(\frac{\sigma}{r_{cut}}\right)^{12} - \left(\frac{\sigma}{r_{cut}}\right)^{6}$, which corrects for the discontinuity of the potential at $r = r_{cut}$.

ESPResSo allows for explicit bonds between specified particles. Adjacent particles can be combined via 2-body spring potential, 3-body angular potentials and 4-body dihedral potentials.

Figure 1(a) shows the 2-body spring bond (harmonic bond) potential given by

$$U_{harmonic-bond} = k(r_{ij} - r_0)^2, \tag{2}$$

where $r_{ij} = \|\vec{r}_j - \vec{r}_i\|$ gives the distance between the particles, r_0 is the equilibrium distance, and k is the spring constant. This potential describes the vibrational motion between an (i, j)-pair of bonded particles. Another 2-body potential is the rubber-band-like, symmetrical FENE-bond (finite extension nonlinear expander) potential given by

$$U_{fene-bond} = -\frac{1}{2}k\Delta r_{max}^2 \ln[1 - (\frac{r - r_0}{\Delta r_{max}})^2], \tag{3}$$

where Δr_{max} is the maximal stretching out of the equilibrium bond length r_0.

The 3-body angular bond is used to fix the angle between the vectors from the center particle to the two other particles (Fig. 1(b)). The energy configuration of the angular bond potential is

$$U_{angle} = k_\theta(\theta - \theta_0)^2, \tag{4}$$

where θ is the angle in radians between vectors $\vec{r}_{ij} = \vec{r}_j - \vec{r}_i$ and $\vec{r}_{kj} = \vec{r}_j - \vec{r}_k$, θ_0 is the equilibrium angle, and k_θ is the angle constant.

Figure 1(c) shows the dihedral potential that describes the angular spring between the planes formed by the first three and last three atoms of a consecutively bonded (i, j, k, l)-quadruple of particles. Then, the dihedral potential is given by

$$U_{dihedral} = k(1 - \cos(n\phi - p)), \tag{5}$$

where n is the multiplicity of the potential and can take any integer value (typically from 1 to 6), p is a phase parameter and k is the bending constant of the potential. ϕ is the dihedral angle between the particles defined by the particle quadrupel p_1, p_2, p_3 and p_4, i.e. the angle between the planes defined by the particle triples (p_1, p_2 and p_3) and (p_2, p_3 and p_4).

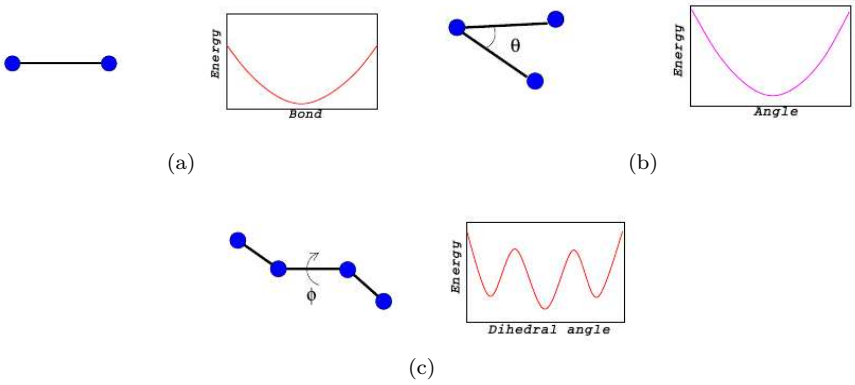

Figure 1: Bonded potentials: (a) 2-body spring bond potential , (b) 3-body angular bond potential, and (c) dihedral potential

2.2 Numerical Solver

The Langevin equation of motion is used to model the particle motion including Brownian motion. At each time step all particles are subjected to a random force and a frictional force such that these two forces satisfy the fluctuation-dissipation theorem and balance each other. In this formalism, the Langevin equation for the i-th particle is given by

$$m\dot{u}_i(t) = -\gamma F_C + W_i(t), \tag{6}$$

where F_C are conservative forces, $\gamma = \zeta/m$ is the friction constant per unit mass between the primary particles and surrounding fluid, u_i is the velocity of the i-th particle and $W_i(t)$ is Einstein's white noise term, which is a Gaussian random source [9,10]. The noise models the random kicks of the fluid molecules to the particles with zero-mean and satisfies,

$$< W_i(t) >= 0 \qquad\qquad \langle W(t)W(t')\rangle = \delta(t-t'). \tag{7a}$$

The friction coefficient, ζ is the proportionality constant between the drag force and the relative velocity between the particle and surrounding fluid. It can easily be seen from Eqn. (8) that the drag force and thus the friction coefficient are proportional to a fluid property (via fluid property, viscosity μ_f and a particle property, particle diameter d_p). The exact modeling of the friction coefficient may also depend on the Knudsen number Kn, which is the ratio of the fluid molecules mean free path length l_{fluid} to the particle radius, $K_n = 2l_{fluid}/d_p$ [11]. For large particles ($Kn << 1$), the flow is in the continuum regime and the well known Stokes law applies,

$$\zeta = 3\pi\mu_f d_p m. \tag{8}$$

For smaller particles ($Kn > 1$), however, a slip velocity between the particle and the surrounding fluid will exist, the friction coefficient will be lower than the Stokes law would predict and the so-called Cunningham correction, C_C needs to be introduced as is indicated by equations (9a) and (9b) [12],

$$\zeta = \frac{3\pi\mu_f d_p m}{C_C} \tag{9a}$$

$$C_C = 1 + K_n \left(A_1 + A_2 \cdot \exp\left[\frac{-2A_3}{K_n} \right] \right). \tag{9b}$$

2.3 Units

In MD simulations, we use "reduced units" or dimensionless variables. Three reference quantities define the unit system, the units of energy (ϵ^*), length (σ^*) and mass (m^*). All other quantities such as temperature, time, and pressure are expressed in units that can be derived from (ϵ^*), (σ^*) and (m^*) by dimensional analysis (Eqn. (10)).

The reference time scale and temperature are given by

$$\text{reference time: } \tau^* = \sigma^*(m^*/\epsilon^*)^{1/2} \tag{10a}$$

$$\text{reference temperature: } T^* = \epsilon^*/k_B \tag{10b}$$

The reference values of energy, mass and length are set to the thermal energy of the system ($\epsilon^* = 3/2\ kT$), the mass of the particle and the diameter of the particle, respectively.

The normalized key quantities of the MD simulation are then given by

$$\text{normalized distance: } \widetilde{r} = r/\sigma^* \tag{11a}$$

$$\text{normalized energy: } \widetilde{E} = E/\epsilon^* \tag{11b}$$

$$\text{normalized temperature: } \widetilde{T} = T/T^* \tag{11c}$$

$$\text{normalized time: } \widetilde{\tau} = \tau/\tau^* \tag{11d}$$

The time step (τ) of the MD simulations plays important role in solving the equation of particle motion. It should be as large as possible to still get accurate tracejtories, conserve energy and reduce requirements for computer time. To obtain reliable simulations, the simulation time step should be much smaller than the relaxation time of the particles, which is the characteristic time for a particle to transit from one state to another state. The relaxation time of a Brownian particle is given by,

$$\tau = \frac{m}{\gamma} = \frac{\rho d^2 C_C}{18\mu}. \tag{12}$$

2.4 Simulation Parameters

In this study, the simulations are carried out with a system consisting of spherical Lennard-Jones particles with a density of $\rho = 1300\ kg/m^3$ in a cubic box with periodic boundary conditions for all sides. The surrounding fluid is assumed to be air with viscosity of $\mu = 1.98310^{-5}\ kg/ms$. The other simulation parameters for the different simulation cases are listed in Table 1. For all simulations, the canonical ensemble is assumed, where the number of particles N, the volume V and the temperature T are fixed.

Table 1: Simulation parameters

	Cross-Shape Test	Square Shape Test	Randomly Placed Particles Test	Effect of Brownian Motion Test
Normalized Time Step	0.0001	0.0001	0.0001	0.005
Number of Particles	17	16	500	1000
Normalized system friction/temp $\widetilde{\gamma}/\widetilde{T}$	1	1	1	16.4-6.8-3.9
Normalized Lennard-Jones Parameters	ϵ=1 σ=1 r_{cut}=2.5σ	ϵ=1 σ=1 r_{cut}=2.5σ	ϵ=1 σ=1 r_{cut}=2.5σ	ϵ=1 σ=1 r_{cut}=2.5σ
Normalized Box Length	36σ	36σ	40σ	100σ
Case Names	Case-1	Case-2	Case-3	Case-4

2.5 Particle Agglomeration Models

The physical and chemical processes behind the particle sticking are natural adherence forces that bring the particles together and/or chemical bonds. When the particles meet, they either feel a short-range attraction (that arises because of the induced-dipole forces) that results in an elastic deformation leading to a flattening of the particles in the contact region and thus strengthens the contact, or they create bridges from one particle to another. However, spherically symmetric interactions are not capable of modeling the physical process of sticking particles, since this requires particle deformations, in which the particles are not in spherical shape anymore. Despite this fact, MD can *model* the sticking of particles by introducing intermolecular or bonded potentials, or binding agents that Espresso package provides.

In the present study five different models are developed to simulate the simultaneous formation and growth of agglomerates. They are summarized in Table 2.

Table 2: Summary of the five different agglomeration formation models

Model Number	Model Name	Model Description	Acronym
i	Lennard Jones model	collision model with highly attractive Lennard Jones potential	LJ
ii	Single bond model	single bond potential between collided particles model	SB
iii	All bonds model	single bond, angle and dihedral potentials model	AB
iv	Single bonded virtual sites model	collision model with two virtual particles at the contact point and connected by a spring bond	SBV
v	Angle bonded virtual sites model	collision model with two virtual particles connected through angle potential	AnBV

For all these models, the particle-particle connections are created dynamically during the simulations when particles come into contact, but the method, how these particles are joined, are different.

2.5.1 Model using highly attractive Lennard Jones potential (LJ)

In this model, the particles interact by highly attractive Lennard-Jones potential forces. If particles come close, the strong attraction makes it very unlikely that they separate again. However, the interactions are still rotationally invariant. For the LJ model simulations, the σ and ϵ values are set such that for small distances between the two particles highly attractive forces act on both particles. These forces can be expressed by Equation (1).

2.5.2 Single bond model (SB)

For the "single bond" model, a distance-dependent bond potential (i.e. harmonic or fene potential) is used to connect the colliding particles.

2.5.3 All bonds model (AB)

The "all bonds" model uses the 3-body angular bond and dihedral bond potentials to represent the adhesion of the particles in addition to the 2-body potential.

2.5.4 Single bonded virtual particles model (SBV)

When, for instance, particles collide and stick together due to local surface effects or chemical bonds, the particles should always be connected at the par-

ticular point where they initially touched. In ESPResSo this can be achieved by using so called virtual particles that are point particles without undergoing any interparticle interactions. They therefore do not have any effect on the particular forces. They can be dynamically created during the simulation, and they move with the Brownian particles they are attached to.

For the "single bonded virtual particles" model, two virtual particles are created at the point of collision, fixed with reference frame of the two collided particles. The virtual particles are bound together by a bond potential with an equilibrium distance equal to zero. In addition, a normal bond is formed between the two collided particles as a control criterion to avoid collision duplication (Fig. 2), and introducing more stiffness of the bond.

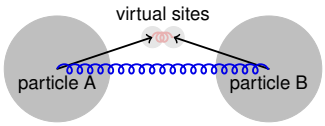

Figure 2: SBV model, collided particles are attached to each other through the virtual particles placed at the collision point.

2.5.5 Angle bonded virtual particles model (AnBV)

Similar to the previous model, two virtual particles are created at the point of contact and the collided particle pair is attached to these virtual particles. However, the virtual particles are connected both to the collided particles and to each other by an angle-dependent potential with angle $\theta = \pi$ as shown in Figure 3.

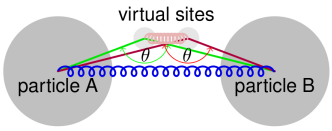

Figure 3: AnBV model, two virtual particles are placed at the collision point and angle potential is defined through two collided particles and virtual particles.

The bond between the centers of the colliding particles prevents significant motion around the point of collision, the angular potential through collided and virtual particles prevents the particles from sliding around each other.

3 RESULTS AND DISCUSSION

Here we present different test cases designed to demonstrate the capabilities of the developed models to simulate the formation and growth of agglomerates in MD (Table 2). First and second cases illustrate the potential existence of the restructuring process within the agglomerates. In order to quantify structural changes we use fractal dimension. The fractal dimensions of the agglomerates are measured from the slope of the log-log plot of the radius of gyration, R_g,

versus the number of particles, N. Taking the logarithms of Witten and Sander's equation [13] given by,

$$N = k_f \left(\frac{R_g}{R_p}\right)^{D_f} \tag{13a}$$

$$\log N = \log k_f + D_f \log R_g - D_f \log R_p, \tag{13b}$$

where k_f is the dimensionless fractal prefactor. It varies depending on the particle number, particle diameter and radius of gyration of the agglomerate. R_p is the primary particle radius.

The radius of gyration of the agglomerates with N particles is the mean root square distance of the particles from the aggregate center of mass, r_0, i.e.

$$R_g = \sqrt{\frac{\sum_{i=1}^{N}(\mathbf{r}_i - \mathbf{r}_0)^2}{N}}, \tag{14a}$$

$$\mathbf{r}_0 = \frac{1}{N}\sum_{i=1}^{N}\mathbf{r}_i. \tag{14b}$$

The computations of Case-1 and Case-2 are used for a direct analysis of the quantitative and qualitative differences between all five models introduced in Section 2.5. In these cases, the initial positions of particles are given with shapes of a cross and square, respectively. The distance between neighboring particles is closer than collision criteria in the simulations. Hence the agglomerates are formed before the iterations start and the initial shape should be preserved.

The normalized time steps of all test case simulations are initially set to $\widetilde{\tau}$=0.01 which is the relaxation time of Brownian particles, (11d) and (12). However, the strong bonds in some systems, especially for the SB and AB models, increases the instabilities and results diverging energy. Thus, the normalized time step is decreased each time one order of magnitude and the simulations are done until they continue without undergoing any program failure. The largest normalized time step values are found to be $\widetilde{\tau}$=0.01 for the LJ, SBV and AnBV, $\widetilde{\tau}$=0.001 for the SB and $\widetilde{\tau}$=0.0001 for the AB model simulations. $\widetilde{\tau}$=0.0001 was chosen for all models in the Case-1, Case-2 and Case-3 simulations to allow for a fair comparison of results.

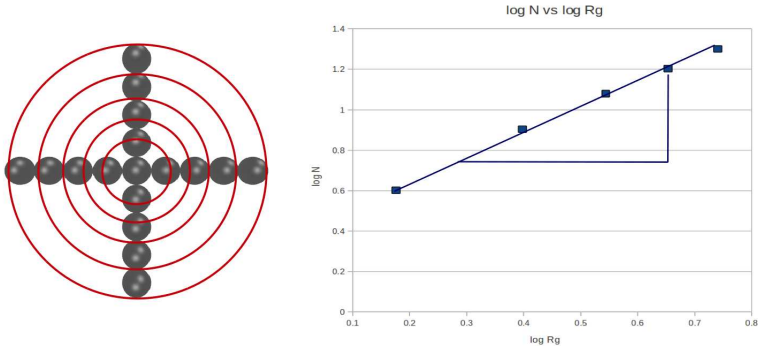

(a) (b)

Figure 4: Fractal analysis of an agglomerate, (a) initially generated cross-shape agglomerate, the concentric circles corresponding to different Rg (b) log-log plot of radius of gyration and particle number

The fractal dimensions of the predefined agglomerates are determined using Equation (13). Figure 4 shows the logarithmic plot of the radius of gyration vs the number of particles in concentric circle for the cross-shaped agglomerate. (The initial fractal dimension of these agglomerates are measured as $D_f = 1.31$ and $D_f = 1.84$ for the cross- and square-shaped agglomerates, respectively.)

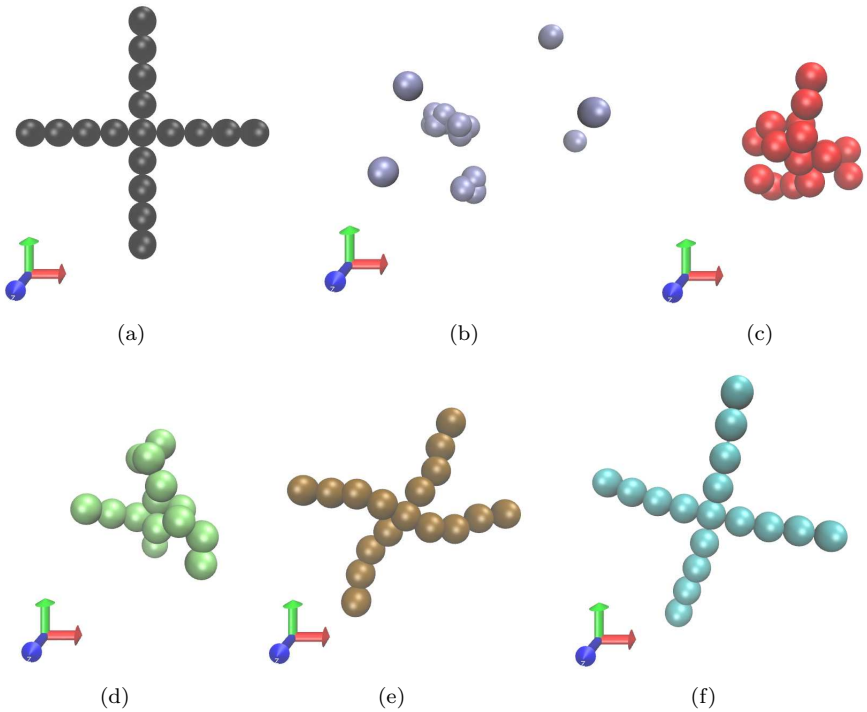

(a) (b) (c)

(d) (e) (f)

Figure 5: (a) The initial configuration of the cross-shaped agglomerate, and its final configurations obtained from (b) LJ model, (c) SB model, (d) AB model, (e) SBV model, (f) AnBV model simulations.

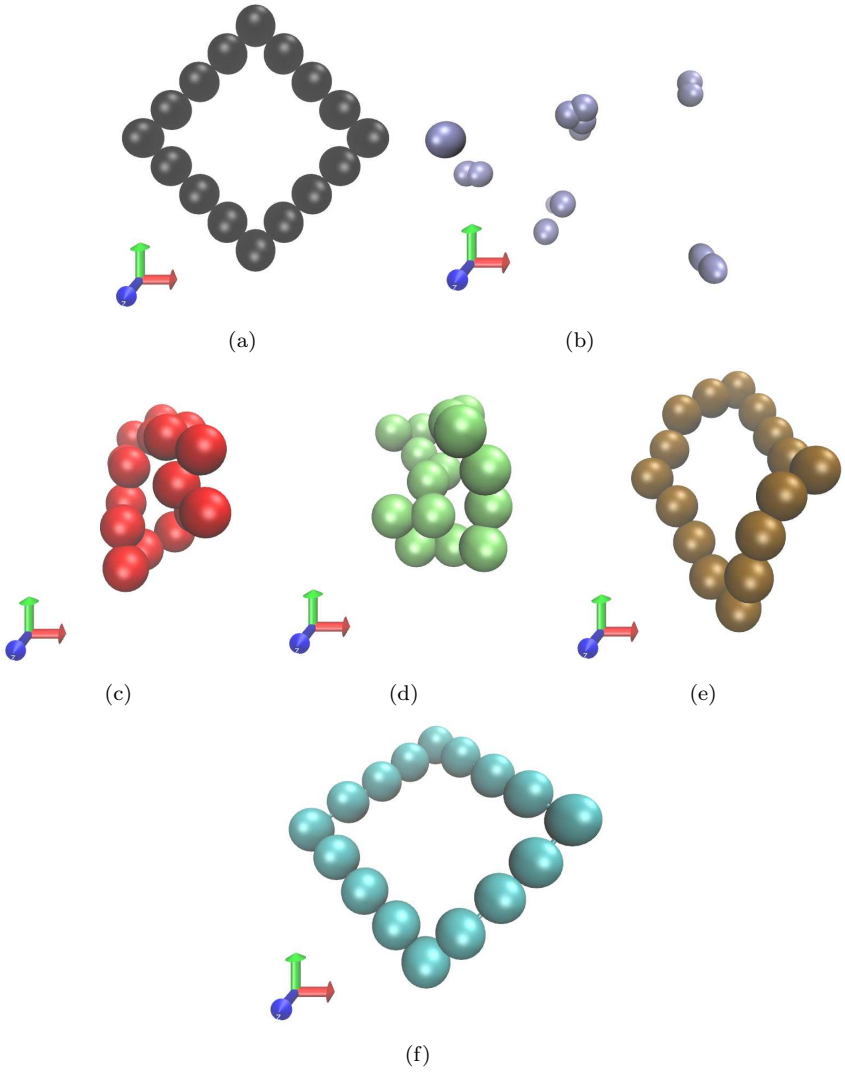

Figure 6: (a) The initial configuration of the square-shaped agglomerate, and its final configurations using (b) LJ model, (c) SB model, (d) AB model, (e) SBV model, (f) AnBV model.

Figure 5 and Figure 6 show the configuration of cross- and square-shaped agglomerates at the end of the simulations using the different models. With the exception of the AnBV model, the agglomerates do not preserve their initial configuration. This is obvious for the LJ, SB and AB models where even the connectivity changes. When using the SBV model, the particles rotate around the connection points within the agglomerates, however, the connectivity is preserved.

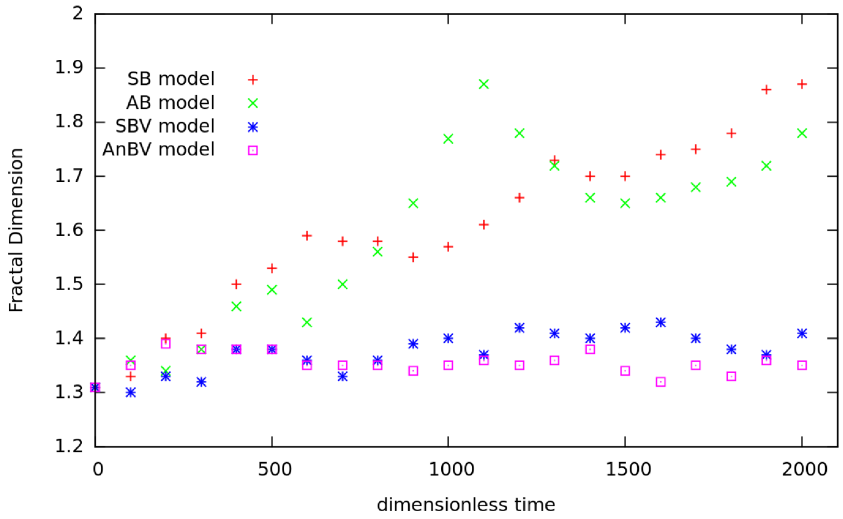

Figure 7: Change in fractal dimension of initially generated cross-shaped agglomeration for different simulation models.

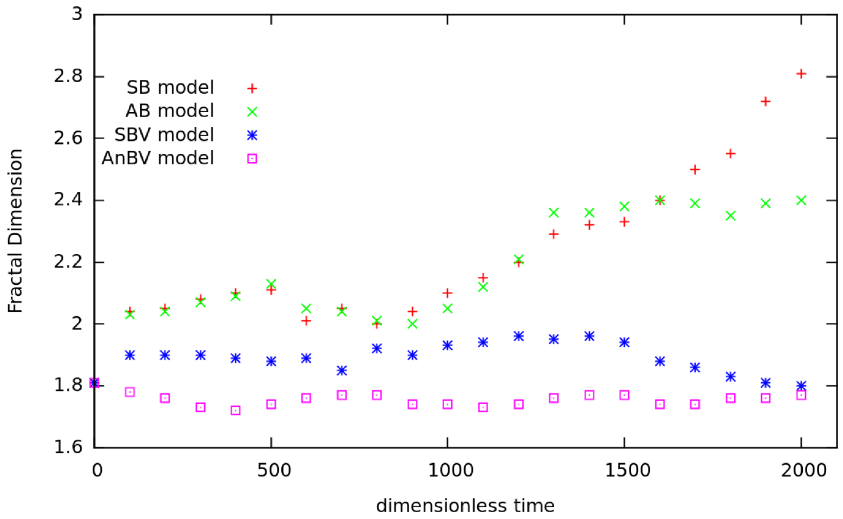

Figure 8: Change in fractal dimension of initially generated square-shaped agglomerate for different simulation models.

The change in the fractal dimension of cross- and square-shaped agglomerates during the Case-1 and Case-2 simulations are reported in Figures 7 and 8 respectively, showing how D_f of each agglomerate varies with time. This change is small in the SBV and AnBV models when compared the SB model and AB model simulations. Moreover, there is no systhematic change in the fractal dimension for the SBV and AnBV models, in contrast to the rest. For

the LJ model, a fractal dimension cannot be defined due to the breakage of the agglomerates.

Further simulations were carried out using increasing attractive potential depth (ϵ) values to avoid breakage in the LJ model.

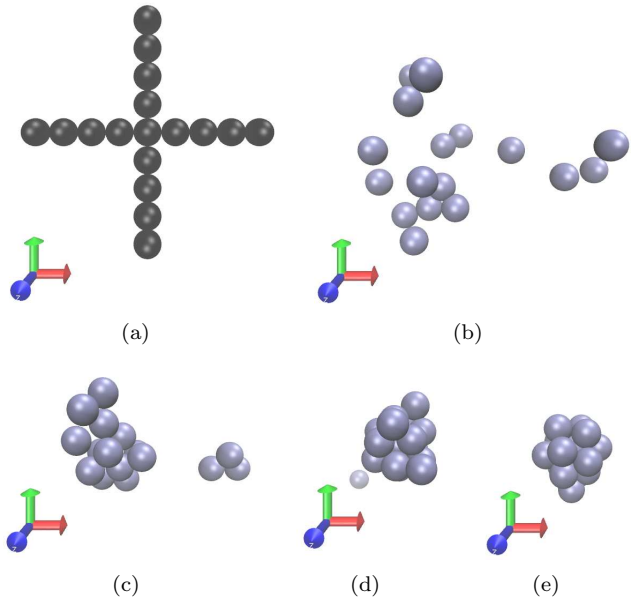

Figure 9: different Lennard Jones attractive potential depth values for LJ-model: (a) The initial configuration of cross-shaped agglomerate, (b) $\epsilon = 1$, (c) $\epsilon = 5$, (d) $\epsilon = 50$, (e) $\epsilon = 500$.

The simulation results indicate that small values of the potential depths cannot avoid breakage while larger ϵ values yield rather compact agglomerates that do not preserve the initial shape, shown in Figure 9.

The obvious changes in the structure of the pre-defined agglomerates simulated by SB and AB models can be correlated with the change in bond length between.

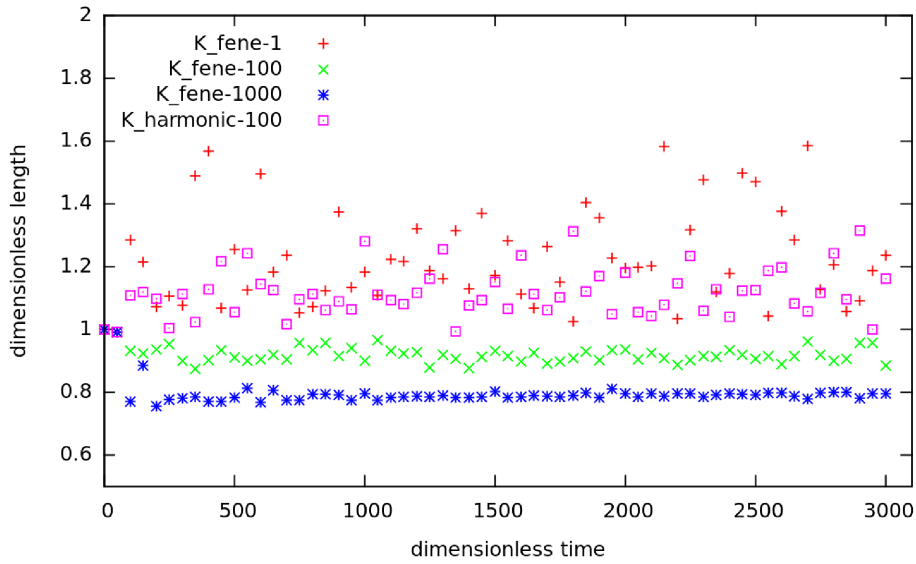

Figure 10: Change in bond length with different spring bond constants in SB model simulations of square-shape agglomerate.

Figure 10 shows that the 2-body symmetrical spring bond length is changing during the simulation. The distance between the bonded particle pairs reduces when the bond stretching constant increases but can not be remain fixed at the equilibrium value r_0=1σ. Furthermore, bonds do not hold information on the relative orientations of the bonded particles. Therefore the bonded particles can slide around each other and rearrange their positions. As a result, restructuring process arises naturally.

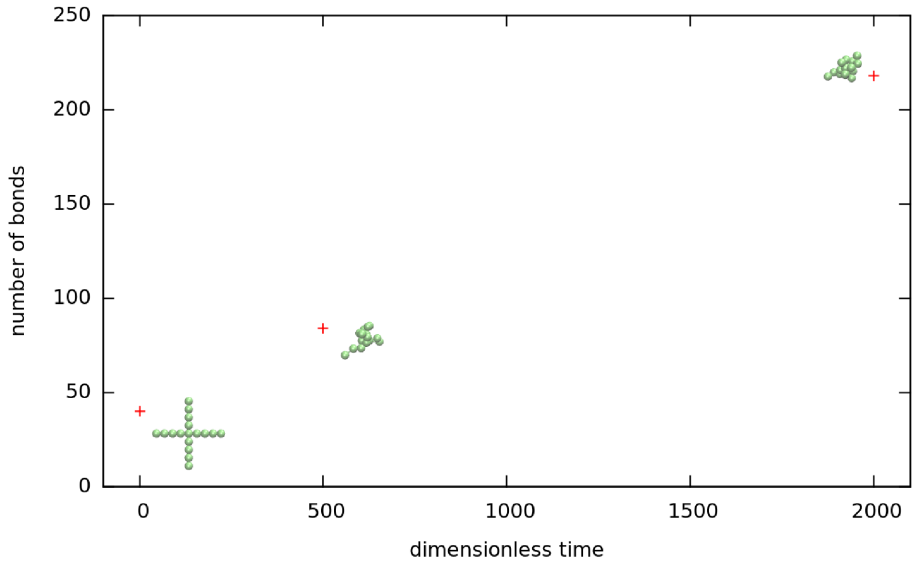

Figure 11: Change in number of bonds during the AB model simulation of cross-shaped agglomerate.

If the particles do not have strong repulsive interactions, this might lead to the formation of further bonds within the cluster, resulting in a rather bulky agglomerate. Figure 11 displays both the number of bonds and the agglomerate shape within the cross-shaped agglomerate during the AB model simulation of Case-1.

The SBV and AnBV model algorithms are more promising for preserving the agglomerate shape and further parameter studies have been performed. The first study reveals the effect of the simulation time step on a known agglomerate structure (Case 1 and Case 2). The second study provides quantitative and qualitative information on the agglomerate structure that are formed from primary particles due to their relative velocity induced by Brownian motion, thereby the differences for the SBV and AnBV models can be identified.

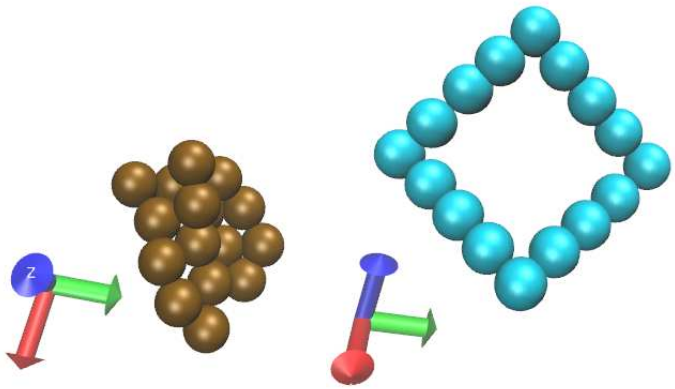

(a) (b)

Figure 12: The final configuration of the square-shaped agglomerate at the end of the simulations of (a) SBV model, (b) AnBV model.

The structures of the square-shaped agglomerate at the end of the SBV and AnBV model simulations are shown in Figure 12. When the normalized time step is increased from τ=0.0001 to τ=0.001 the structure of the square-shaped agglomerate changes dramatically during the SBV model simulation, but for the AnBV model the structure preserves its initial configuration. Additional AnBV model simulations are performed to analyze the sensitivity of the determined agglomerate structure and rigidity to the simulation time step.

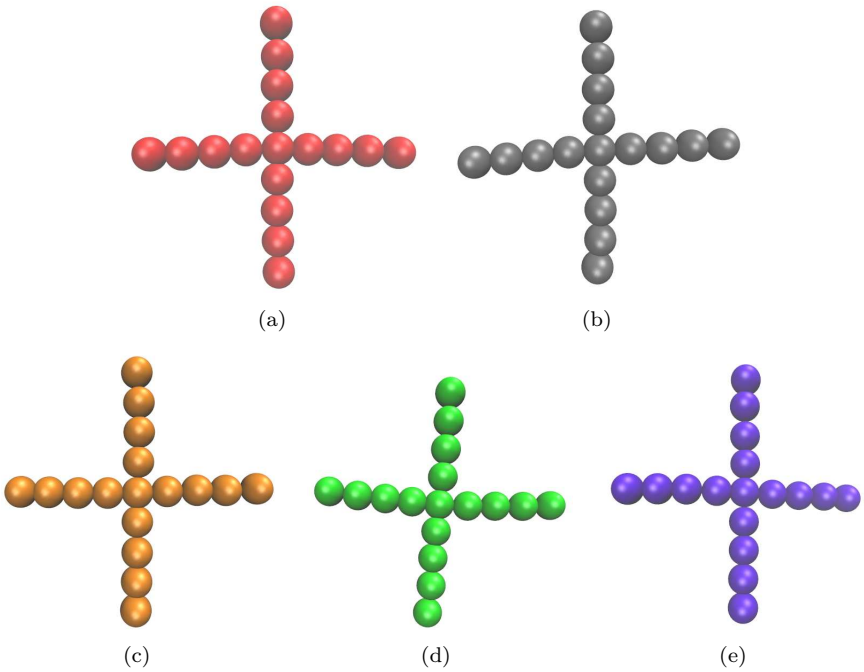

Figure 13: The final configuration of the cross-shaped agglomerate at the end of the AnBV model simulations using different time steps, (a) τ=0.000001, (b) τ=0.00001, (c) τ=0.0001, (d) τ=0.001, (e) τ=0.01.

Figure 13 shows the cross-shaped agglomerate structure during the AnBV model simulations. At different time steps the agglomerate preserves its shape during the simulations. In this respect, the AnBV model gives time step independent results.

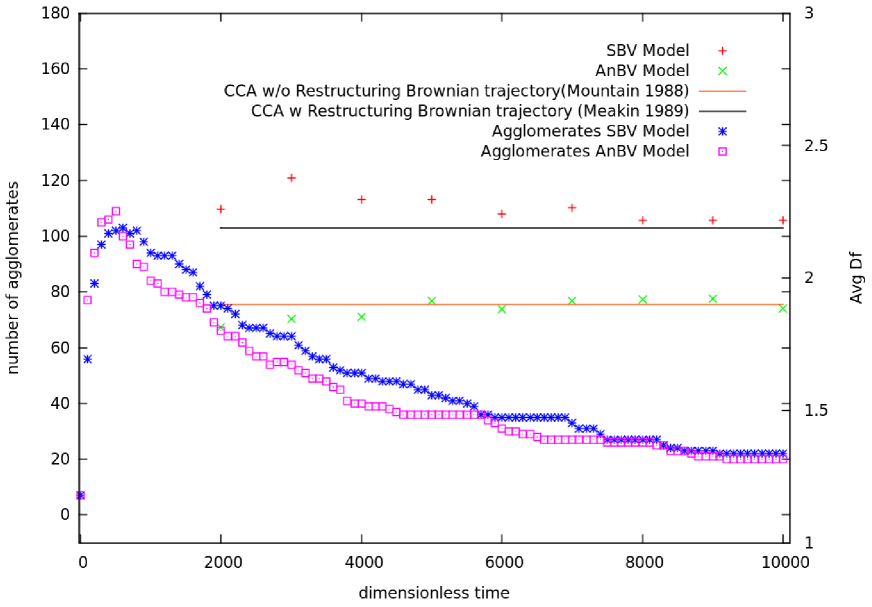

Figure 14: Number of agglomerates and average fractal dimension of the system for SBV and AnBV model simulations.

To assess the difference between the SBV and AnBV models, Case 3 simulations are done. The agglomerates are formed by the collision of single Brownian particles and/or collison of clusters during the simulation. Since the clusters are formed by bonded particles, they move naturally following the same equations as the nano-particles. The agglomeration growth and fractal dimension of formed agglomerates are assessed and shown in Figure 14. At the beginning of the simulations randomly placed 500 particles collide and create clusters, and then with time cluster-cluster collisions form larger clusters. At any time of the computation the average D_f of the agglomerates that are formed in SBV model simulation are higher than the respective values of the AnBV simulation.

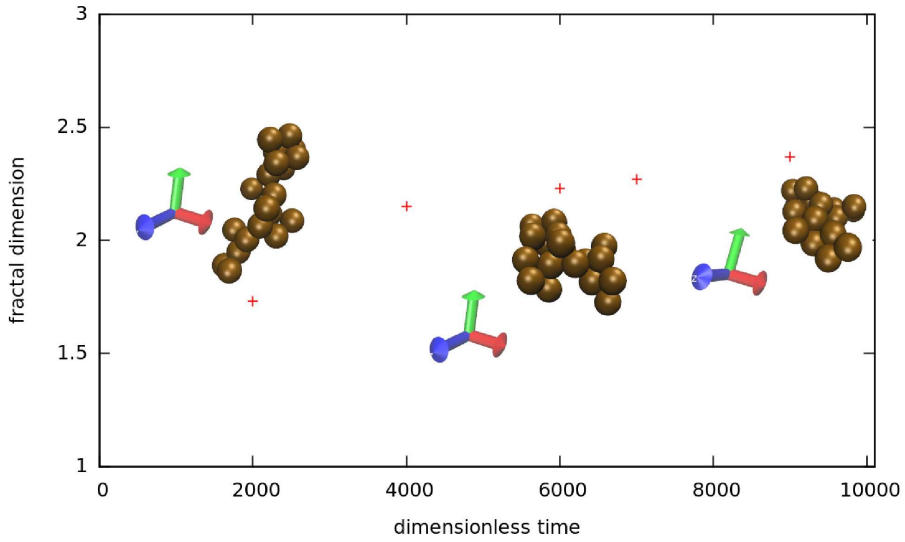

Figure 15: Chenge in structure of a selected agglomerate (N=22) during SBV model simulation of Case-3a.

This can be explained by Figure 15. Here we show the change in the morphology of a selected agglomerate using the SBV model simulation of Case-3. Initially, the agglomerate has D_f=1.74 but a later time the particles reorientate themselves and the number of particle contacts is maximized. This results in a more compact structure with a higher fractal dimension (D_f=2.4 at the end of the simulation).

The mean fractal dimensions vary between D_f=1.8 and D_f=1.9 for the AnBV model simulation and between D_f=2.1 and D_f=2.3 for the SBV model simulation. These values agree well with the numerical studies by Meakin and Jullien [14] and Jullien and Meakin [15] for cluster-cluster aggregates (CCA) grown by diffusion-limited aggregation (DLA) including impact restructuring. In their studies, the aggregates might fold, bend and twist depending on the allowed restructuring stages. The fractal dimension was found as D_f=1.80 for no-restructuring case and it increased to D_f=2.09 if the agglomerates were allowed to bend, to D_f=2.17 if both bending and folding were allowed and to D_f=2.19 if the complete restructuring stages were included for CCA aggregates grown by DLA.

The last test was done to investigate the effect of Brownian motion on cluster-cluster agglomerates modeled by the AnBV algorithm. Different values are defined for the diffusion coefficient, $\widetilde{\gamma}/\widetilde{T}$ parameter which affects the Brownian motion as shown by Equations (6) and (9). At smaller temperatures, the particles move slower as the effect of friction is more dominated compared to the impact effect of fluid molecules, therefore the ratio ($\widetilde{\gamma}/\widetilde{T}$) is high (i.e. at 300K $\widetilde{\gamma}/\widetilde{T}$=16.45). Case-4 illustrates the formation and growth of agglomerates from randomly placed 1000 Brownian particles.

The number of particles in all clusters for the Case-4 simulations are plotted in Figure 16 together with the number of clusters formed at every 100 iterations.

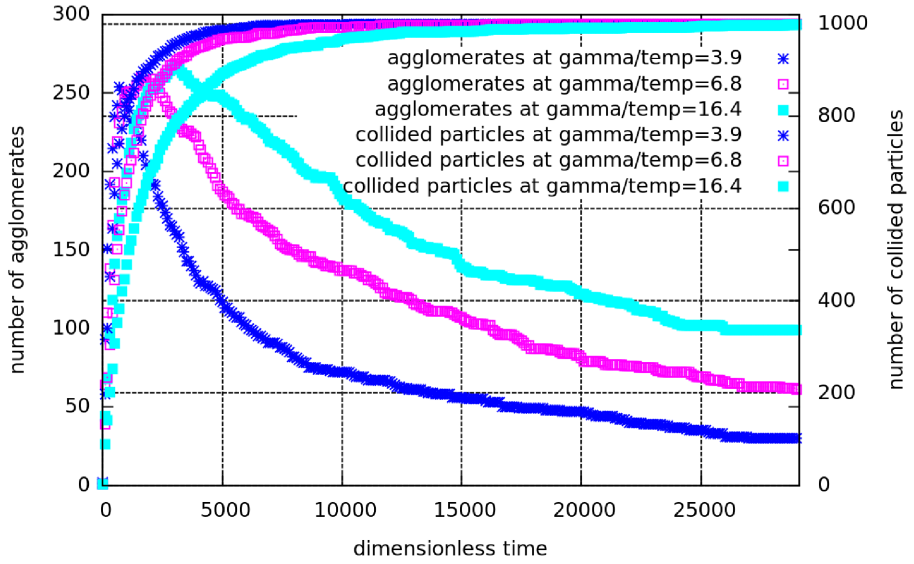

Figure 16: Number of collided particles and agglomerates change at 3 different ratios.

Simulation results indicate that the cluster formation and cluster growth speeds are high at lower ratios as the particles move fast and thus the collision probability is high. At $\widetilde{\gamma}/\widetilde{T}$=3.9, the aggregate formation from particle particle collisions is completed after the first 500 iterations and then the particle-cluster and cluster-cluster agglomerates start forming. At $\widetilde{\gamma}/\widetilde{T}$=16.4, the particles and as well as the agglomerates move slower, therefore the agglomeration process is slower compared to other simulations.

Table 3: Average fractal dimension

Normalized time/avg. Df	16.4	6.8	3.9
1000	–	–	1.82
20000	–	1.77	1.77
47000	1.72	–	1.745
52000	–	–	1.73

The fractal dimension values of formed agglomerates are measured according to logarithmic plot of R_g vs N. The mean D_f values of the $\widetilde{\gamma}/\widetilde{T}$ = 3.9, 6.8 and 16.4 systems at different times but possessing similar agglomerates are summarized in Table 3. The results indicate that the agglomerates formed by the collisions of slowly moving particles have smaller D_f compared to the ones formed by collisions of particles that move faster. Moreover, as the agglomerates grow their fractal dimensions decreases.

4 CONCLUSIONS

In this study, we demonstrated the capability of five different models to simulate the nanoparticle agglomeration process, which require only local bonding. Analyzing the shape and structure of both pre-defined and the randomly formed agglomerates in terms of fractal dimension, it became evident that only the developed AnBV model is capable of modeling nanoparticle agglomeration without undergoing any restructuring process. In our investigations, we found that using only non-bonded interactions (LJ model) is not sufficient to hold particles together and prevent sliding around contacts. Also the SB and AB models including bonded potentials do not hold the particles at the contact point and allow restructuring. Hence, only bulky and compact agglomerates are formed. Also during the simulations, the large number of formed bonds increases the system energy and thus limits the time step. Our SBV model prevents restructuring but particles can fluctuate considerably around the connection point. Performing different AnBV model simulations using different time steps, the results indicate that this model can avoid restructuring at large time steps. Furthermore, the AnBV model simulations of cluster cluster agglomerates obtained by collisions of randomly placed Brownian particles were investigated. The fractal dimensions of analyzed agglomerates are in good aggreement with other simulations and experiments. Finally from the present detailed simulations, it is found that the larger clusters have smaller fractal dimension values.

5 FUTURE WORK

Further simulations will be performed using AnBV model to analyse the agglomeration efficiency determined by the sticking of collided particles due to both Brownian motion and the shear flow. Advanced long-term goal is the coupling the flow field with the particle transport and the agglomerate transport to determine the impact of turbulent convection on agglomerate formation, growth and transport.

References

[1] T. Kodas, M. Hampden-Smith, Aerosol processing of of materials, WILEY-VCH, Weinheim, 1999.

[2] J. Gregory, Particles in water: Properties and processes, CRC Press, USA, 2005.

[3] L. Zaichik, V. Alipchenkov, E. Sinaiski, Particles in turbulent flows, WILEY-VCH, Weinheim, 2008.

[4] S. Das, S. Garrick, The effects of turbulence on nanoparticle growth in turbulent reacting jets, Advances in Colloid and Interface Science 97 (2002) 151–177.

[5] M. Babler, J. Sefcik, M. Morbidelli, J. Baldyga, Hydrodynamic interactions and orthokinetik collisions of porous aggregates in the stokes regime, Physics of Fluids 18 (2005) 013302.

[6] M. Sander, R. Patterson, A. Raj, M. Kraft, On the fractal dimension of soot particles (2009).

[7] M. Vanni, G. Baldi, Coagulation efficiency of colloidal particles in shear flow, Advances in Colloid and Interface Science 97 (2002) 151–177.

[8] H. Limbach, A. Arnold, B. Mann, C. Holm, Espresso an extensible simulation package for research on soft matter systems, Comput. Phys. Commun. 174 (2006) 704–727.

[9] R. Fox, Gaussian stochastic process in physics, Physics Reports 48 (1978) 179–283.

[10] D. S. Lemons, Paul Langevin's 1908 paper: On the theory of brownian motion, C. R. Acad. Sci. 146 (1908) 530–533.

[11] C. Hogan, Fractal aggregate coagulation with primary particles in the presence of interparticle particle forces, Aerosol Science and Technology.

[12] K. Lee, H. Chen, Coagulation rate of polydisperse particles, Aerosol Science and Technology 3 (1984) 327–334.

[13] C. Xiong, S. Friedlander, Morphological properties of atmospheric aerosol aggregates, Proceedings of the National Academy of Sciences 98 (2001) 11851–11856.

[14] Z. Chen, P. Weakliem, P. Meakin, Hydrodynamic radii of diffusionlimited aggregates and bondpercolation clusters, J. of Chem. Phys.

[15] R. Jullien, P. Meakin, Simple models for the restructuring of three-dimensional ballistic aggregates, J. Colloid and Interface Science 127 (1989) 265–272.